



# Moisture and salinity profiles in the French Atlantic coastal marshes and consequences on plant available water

Raymond Tojo Radimy, Patrick Dudoignon, Laurent Caner, Jean-Michel Hillaireau

## ► To cite this version:

Raymond Tojo Radimy, Patrick Dudoignon, Laurent Caner, Jean-Michel Hillaireau. Moisture and salinity profiles in the French Atlantic coastal marshes and consequences on plant available water. Journal of Hydrology: Regional Studies, 2017, 9, pp.1 - 17. 10.1016/j.ejrh.2016.11.002 . hal-01724407

HAL Id: hal-01724407

<https://hal.science/hal-01724407>

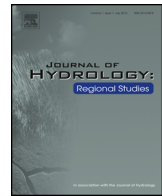
Submitted on 23 Sep 2021

**HAL** is a multi-disciplinary open access archive for the deposit and dissemination of scientific research documents, whether they are published or not. The documents may come from teaching and research institutions in France or abroad, or from public or private research centers.

L'archive ouverte pluridisciplinaire **HAL**, est destinée au dépôt et à la diffusion de documents scientifiques de niveau recherche, publiés ou non, émanant des établissements d'enseignement et de recherche français ou étrangers, des laboratoires publics ou privés.



Distributed under a Creative Commons Attribution 4.0 International License



## Moisture and salinity profiles in the French Atlantic coastal marshes and consequences on plant available water



Raymond Tojo Radimy<sup>a</sup>, Patrick Dudoignon<sup>a,\*</sup>, Laurent Caner<sup>a</sup>,  
Jean-Michel Hillaireau<sup>b</sup>

<sup>a</sup> University of Poitiers - ENSIP, IC2MP-HydrASA UMR 7285, 1 rue M. Doré, TSA 41105, 86073 Poitiers, France

<sup>b</sup> INRA - Domaine Expérimental St Laurent de la Prée. 17450 St Laurent de la Prée, France

### ARTICLE INFO

#### Article history:

Received 10 February 2016

Received in revised form 2 November 2016

Accepted 3 November 2016

Available online 22 November 2016

#### Keywords:

Clay dominated soils  
Coastal marshlands  
Plant available water  
Hydric stress  
Salt stress

### ABSTRACT

**Study region:** French Atlantic coastal marshlands.

**Study focus:** These coastal marshes have been reclaimed from the sea by successive polderizations since the Middle Ages. The soils have been formed by desiccation, consolidation and maturation of clay-dominated sediments initially saturated by seawater. Since the 1970's the extensive cultivation of grain was accompanied by widespread drainage in order to deepen the groundwater level and increase the thickness of surface leaching by rainfall. Gravimetric water and salinity profiles were recorded in an undrained grassland and a drained cornfield profiles during the period of corn plant growing from July to September 2013. The simple available water capacity (AWC) calculation from surface parameters were compared to vertical profiles of plant available water (PAW). The limit between the vadose and saturated zones was determined by comparison between the shrinkage and compaction pathways of the clay matrix. Patterns of the PAW profiles were calculated and modeled following simple second-degree polynomial equations.

**New hydrological insights for the region:** The results demonstrate the PAW evolution at successive depths compared to deepening evapotranspiration drying fronts and ascending capillarity rise. Based on soil water contents measured at 10 cm and/or 20 cm depths, the modeled PAW profiles are found sufficiently realistic to be used as an efficient tool to aid crop farming in these territories governed by the superimposed water and salt stresses.

© 2016 The Authors. Published by Elsevier B.V. This is an open access article under the CC BY-NC-ND license (<http://creativecommons.org/licenses/by-nc-nd/4.0/>).

## 1. Introduction

The coastal marshlands have been generally reclaimed from primary fluvio-marine sediments. They result from hydraulic managements and/or polderization that may date from the Middle Ages. Historically these hydraulic managements were built for reasons of sanitation, breeding and farming. For the intensive grain crops the slow drying caused by land reclamation

**Abbreviations:** AWC, available water capacity equivalent to the difference between the water content at wilting point and water content of retention capacity (field capacity); AWC<sub>ref</sub>, available water capacity calculated from soil texture used as reference in the work; PAW, plant available water calculated taking into account the real water content of soil for the different dates; PE and ET<sub>m</sub>, potential and maximum evapotranspiration; RR, rainfall; W, gravimetric water content; W<sub>s</sub>, W<sub>p</sub>, W<sub>l</sub>, shrinkage plasticity and liquidity limits; W<sub>fc</sub>, field capacity; W<sub>wp</sub>, wilting point; EC<sub>1/5</sub>, 1/5 electrical conductivity; K<sub>c</sub>, crop coefficients; K<sub>s</sub>, hydraulic conductivities at saturation; AEP, air entry point; GWET, groundwater evapotranspiration; VZET, vadose zone evapotranspiration.

\* corresponding author.

E-mail addresses: [raymond.tojo.radimy@univ-poitiers.fr](mailto:raymond.tojo.radimy@univ-poitiers.fr) (R.T. Radimy), [patrick.dudoignon@univ-poitiers.fr](mailto:patrick.dudoignon@univ-poitiers.fr) (P. Dudoignon), [laurent.caner@univ-poitiers.fr](mailto:laurent.caner@univ-poitiers.fr) (L. Caner), [jean-michel.hillaireau@stlaurent.lusignan.inra.fr](mailto:jean-michel.hillaireau@stlaurent.lusignan.inra.fr) (J.-M. Hillaireau).

was recently improved by drainage. The primary sediments were generally saturated by salt water, thus, the current water table and deepening desiccation front cause synchronous evolutions of the water content and salinity profiles. In these shallow groundwater regions the capillary rise may have dominant roles in the mechanisms of plant-soil interaction, such as soil water flux, crop rooting and water salinity (Ayars et al., 2001, 2006a, 2006b). The shallow groundwater may have a positive role on plant growth via water supply and/or a negative role via waterlogging or salinization (Nosesto et al., 2009). Crops also influence the water and salinity profiles, and consequently the groundwater level via the PE or ETm balances (Fan et al., 2014).

One can explain that plant growth and crop yields are partly governed by the soil AWC and secondly by the water content and associated PAW profiles with soil depth. AWC is commonly calculated from the soil texture (clay/silt ratio) and/or from the difference between the water content at field capacity and at wilting point (Bruand et al., 1996; Rawls et al., 1982; Mathieu and Pielat, 1998; Saxton and Rawl, 2006). Such calculated AWC is a basic parameter characteristic of the potential (maximum) of water retention by the soil which can be used as a reference but which is independent of weather conditions and the water consumption of plants. This AWC may be upgraded by taking into account the rainfall (RR), the potential of evapotranspiration (PE) and the crop coefficient (Kc) in the  $AWC_{PE}$  or  $AWC_{ETm}$  calculations for grassland and grain crops, respectively. In fact, plant growth and crop yields are mainly governed by soil moisture profiles and the evolution of the PAW profile throughout the seasons. Firstly, the PAW changes according to seasonal variations of the water profiles resulting from the competition between the rainfall and PE or ETm. Secondly, in shallow groundwater fields the PAW is largely supplied by the groundwater capillary rise. Numerous simulations of water flux in saturated and vadose zones have been conducted since the 2000s' (Guber et al., 2009). The difficulties of modeling are in part due to difficulties in the measurement of the water retention and hydraulic conductivity of clayey soils. They are also due to the nonlinear hydraulic properties of the upper vadose zone. The amount of parameters to be considered led to the development of a multi-model prediction in 1969 (Bates and Granger, 1969). The pedotransfer functions have largely been developed but the challenge is to fit the models to the different fields, crops and soils. For different studied fields, the question is: how to adapt a multi-model to the *in situ* available parameters, and can a simple model be realistic enough for crop farming?

Generally, the soils of the coastal marshlands have two dominant features:

- a silty-to-clay dominated texture, inherited from the primary sediments and responsible for drastic properties of shrinkage
- and *in situ* shallow groundwater table, characterized by medium to high salinity.

The clay dominated nature of the soils impacts their hydro-mechanical properties and water fluxes through the changing micro-to-meso structure of the clay matrix from the surface to the depth (Archer and Smith, 1972; Kern, 1995a,b; Saxton and Rawls, 2006; Bernard et al., 2007; Bernard-Ubertosi et al., 2009; Gallier et al., 2012). Indeed these clayey soils present important shrinkage/swelling properties depending on water content. Furthermore, because of close mineralogy and texture they always present the same gravimetric water contents (W) at the characteristics shrinkage ( $W_s$ ), plasticity ( $W_p$ ) and liquidity ( $W_l$ ) limits. From the surface to the depth, the gravimetric water content increases due to the presence of a shallow water table and capillary rise. As a result, according to the progressive increase of W with depth from the surface to the depth the clay matrix presents solid state pathways from shrinkage limit ( $W_s$ ) to plasticity limit ( $W_p$ ) and plastic state pathways from  $W_p$  to liquidity limit ( $W_l$ ) (Fig. 1a). The depth at which these changes ( $W_s$  to  $W_p$  to  $W_l$ ) occur is an important parameter for the hydromechanical behavior of the soil and the associated water content profiles. Decreasing the size of micropores according to the desiccation/shrinkage phenomenon decreases the capillary rising rate but increases the height of capillary fringe (Fig. 1b). The shallow silty-clay aquifers suggest a large groundwater recharge by capillary rise in response to the evapotranspiration flux (Ayars et al., 2006a,b; Fan et al., 2014).

In parallel, regarding the capillary fringe, plant growth and rooting depth are also governed by the thickness of the vadose zone, groundwater saturated zone and water table level. In such clay dominated soils and shallow salty groundwater, the competition between evapotranspiration and groundwater supply governs the water content profiles and the hydric stress plus salt stress combine. The kinetics of the water profile evolutions are partly governed by the associated clay matrix micro-to-meso structure (shrinkage/swelling) and water table level. During the last twenty years, many authors have used pedotransfer functions at the scale of soil profiles in order to link the prevailing weather conditions, the rooting depths and the crop coefficients (Nosesto et al., 2009; Guber et al., 2009; Bastet et al., 1998; Bruand et al., 2002, 2004; Morvan et al., 2004; Bruand and Coquet, 2005; Choisnel, 1992; Nyvall, 2002; Hong et al., 2013). In such shallow, silty-to-clay groundwater territories the question is also how to monitor the saturation front and consequently how to quantify groundwater evapotranspiration and vadose zone evapotranspiration (Ayars et al., 2006a,b; Shah et al., 2007). More recently, the definition of soil water availability has been broadly discussed regarding the transpiration demand and root development of plants (Couvreur et al., 2014). Thus, works on the soil water stress function suggest a "limited soil water availability" depending on plant potential transpiration rate and root water uptake evolution: i.e. hydrodynamics of the soil-plant system (Javaux et al., 2013). In fact, the root water uptake depends on both a three-dimensional root network and surrounding clay matrix hydraulic conductivity. Moreover, the mechanisms are also disturbed by heterogeneities at the root-soil interfaces. Root growth provokes the rearrangement of clay particles along the root surface through mechanical and desiccation stresses on the clay matrix. Such "compaction" of the clay matrix drastically decreases hydraulic conductivity (Gallier et al., 2012). In the vadose zone, the soil-root hydraulic resistance may be also impacted by air gaps at the soil-root interface (Carminati et al., 2009). In all cases the AWC,  $AWC_{PE}$  and  $AWC_{ETm}$  are calculated from the "surface conditions" only: i.e. weather including

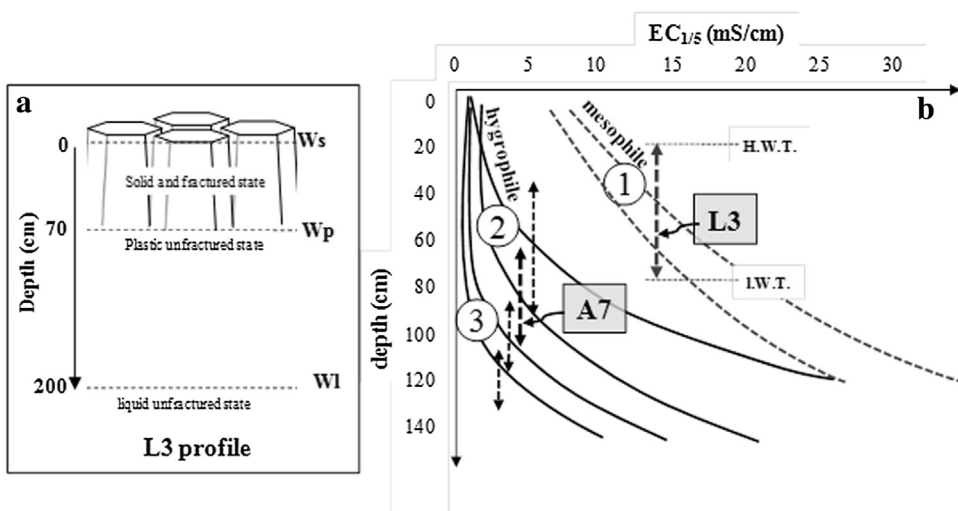


**Fig. 1.** a – Schematic representation of the profile of soil structure (example of L3 grassland), Ws, Wp and WL = shrinkage, plasticity and liquidity limits. b – Representation of the EC<sub>1/5</sub> profiles observed in the INRA site of St Laurent de la Prée, (1) mesophile domain of undrained grasslands, (2) meso-hygrophile domain of drained fields supplied in fresh continental water, (3) hygrophile domain of drained fields distant from the peripheral calcareous hill. The double vertical dash arrows indicate the seasonal amplitude between the high (H.GW) and low (L.GW) groundwater levels. L3 and A7 = hydraulic domains of the studied grassland and drained corn fields respectively (Radimy et al., 2013 modified).

rainfall (RR) and crop coefficients (Kc), and/or a quite homogeneous and stable soil structure. Calculated in mm/m, they only allow representations of simple linear AWC profiles, which are calculated by the multiplication of the AWC<sub>ref</sub> by the depth and by the bulk density of the soil. The PE, ET<sub>M</sub> and RR evolutions provoke only changes in the linear profile slopes (Radimy et al., 2013; 2014). Thus they do not give any indications of the vertical evolution of the PAW profile during plant growth, root deepening and water consumption throughout the season. More realistic representations of the vertical evolution of the AWC profiles have been made, either by considering superimposed layers of soils characterized by their bulk densities and textures or from hydric potential profiles (Braudeau et al., 2005; Bruand and Coquet, 2005). For clay-dominated soils, particularly sensitive to shrinkage, surface desiccation can induce the propagation of shrinkage cracks from the surface down to the level of the hydric potential measurements and disconnect the porous ceramic cups. Thus the water content – soil structure relationship calculated from tensiometer measurements may be unsettled (Radimy et al., 2013).

This paper is based on water and salinity profile monitoring during the 2013 season in undrained grassland and in a drained corn field of the west coast of France located in the INRA experimental site of St Laurent de la Prée (Charente Maritime department, France; Fig. 2). It focuses on the calculation of AWC and PAW profiles of drained and undrained fields. The PAW profiles have to be calculated for successive dates to integrate the vertical moisture profiles, the seasonal PE (or ET<sub>M</sub>) and RR. The evolution of the vadose zone thickness is calculated according to the water content of the Air Entry Point, localized both on the shrinkage curve and compaction curve of the clayey soil-sediment. Predictive modeling of soil/plant interaction in real time requires the calculation of such “residual” PAW profiles regarding the successive stages of plant growth until senescence. In this work we explore the influence of surface conditions (RR, PE, ET<sub>M</sub>, Kc) on the moisture profiles developed in the drained and undrained fields in the shallow salt groundwater. The real PAW profiles are calculated according to the water content profiles. Their evolution through the season, compared to reference AWC<sub>PE</sub> and AWC<sub>ETM</sub>, demonstrates the role of the groundwater capillary rise. The final objective of this paper is to propose a simplified method of “residual” PAW profile modeling that is well adapted to these shallow groundwater coastal marshes and sufficiently realistic to be used as a tool suitable for the hydraulic management of such territories.

## 2. Material and methods

### 2.1. Environmental setting

This study was conducted on the west marshlands located along the Atlantic coast of France (Fig. 2). These territories have been successively reclaimed from seawater and fluvio-marine sediments by drying and polder works since the Middle Ages (from the 11th century to the 17th century). Initially, the sediments were deposited for a period of 8000 years directly onto the Jurassic limestone. The marshes have emerged since the sea regression and were progressively transformed into soils by successive desiccation, consolidation and maturation since at least the 10th century (with the first hydraulic managements). In fact the historical polder management, initially developed for sanitation and breeding, was recently completed by a period of intensive drainage since the 1970s in order to extend the growth area of grain crops. The main role of this drainage is to lower the initial salt groundwater level and, consequently, to increase the thickness of soil surface available for desalinization

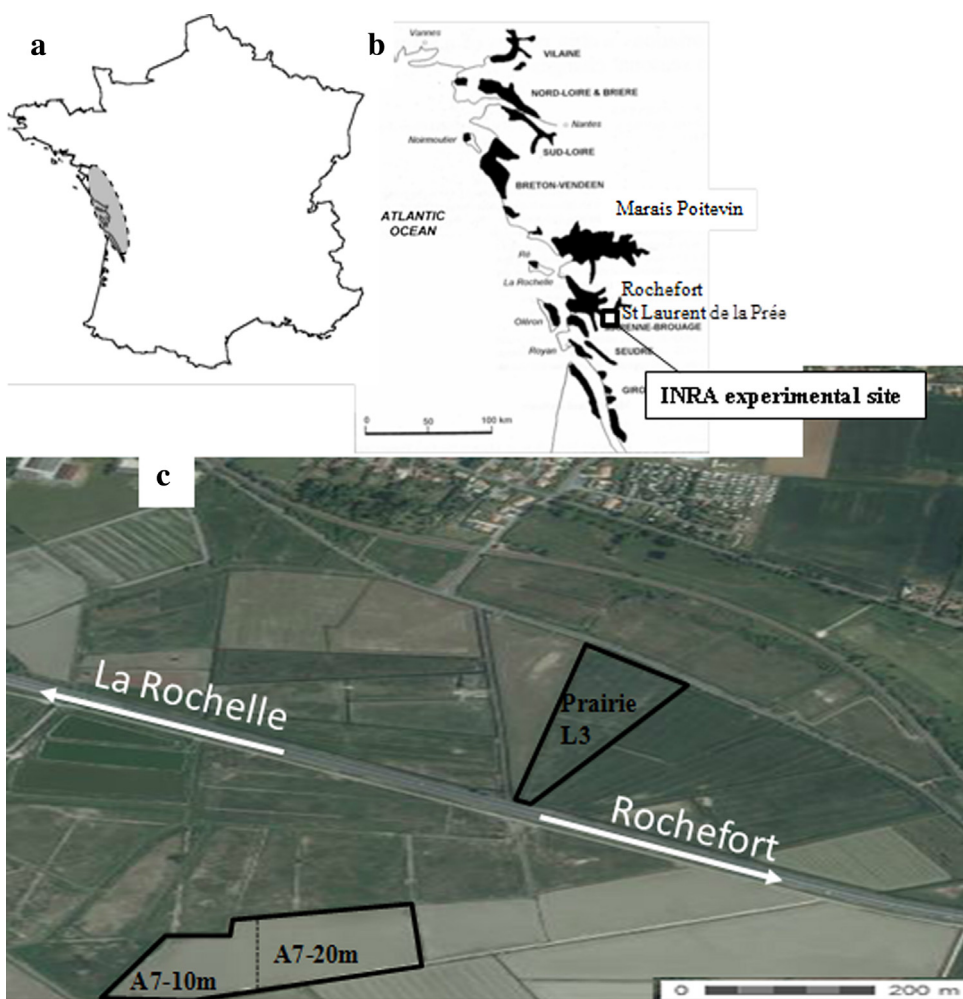


**Fig. 2.** a-Location of the west marsh along the Atlantic coast of France, b-location of the Marais de Rochefort and c- location of the two L3 and A7 fields in the INRA experimental site of St Laurent de la Prée.

**Table 1**

Particle size distribution from the surface to 1.20 m depth. L3–30 cm and A7 – 25 cm characterize the soil surface, A7 120 m a palaeosol layer (Bernard, 2006).

Location	Depth (cm)	<2 µm%	2–5 µm%	5–10 µm%	10–20 µm%	>20 µm%
Grassland	30	11	52	15	14	8
	70	43	19	20	13	5
	120	52	12	15	10	4
A7	25	11	45	18	14	12
	85	55	12	14	13	6
	100	59	12	15	10	5
	120	6	54	21	12	7

by rain leaching. Finally, the flora distribution and the crop fields in the area are governed by hydraulic management and the resulting water-stress and salt-stress combine (Pons et al., 2000; Tournade and Bouzillé, 1991, 1995; Pons and Gerbaud, 2005; Bernard, 2006; Dudoignon et al., 2009; Gallier, 2011; Gallier et al., 2012; Weng et al., 2003; Radimy et al., 2013, 2014). The present work focuses on the INRA experimental site of St Laurent de la Prée located in the “Marais de Rochefort” (Charente Maritime department, France; Fig. 2).

The soils present a silty-to-clay texture with the <20 µm fraction between 85 and 95% and the <2 µm fraction between 40 and 60% except in soil surface (L3–30 cm, A7–25 cm) and in a buried palaeosol (A7–120 cm) where it decreases to 10% (Table 1). The mineralogy is composed of kaolinite, illite, and illite/smectite mixed layers, and a very small amount of pure smectite (Fig. 3). The 0–30 cm layer has a little less clay fraction and lower proportion of smectite (or illite-smectite mixed

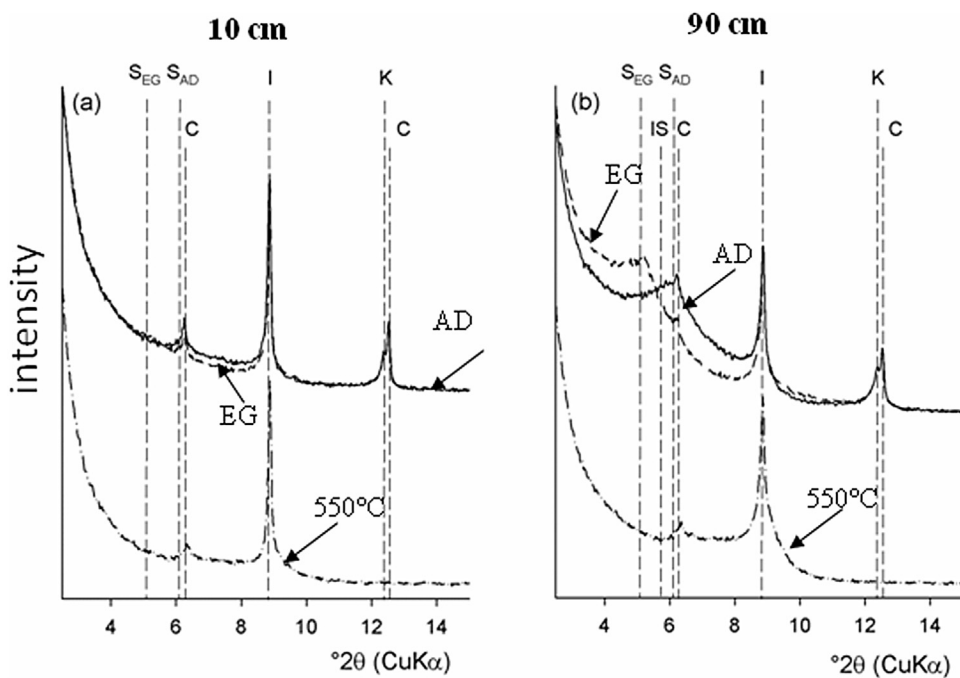


**Fig. 3.** X Ray diffraction patterns of the clay mixture constituting of the soil of L3 field at 10 cm and 90 cm depth. K = kaolinite, I = illite, S = smectite and/or Illite/Smectite mixed layer, black line = AD = air dried, dashed-line = EG = Ethylene glycol solvated, and dash-dotted line = heated at 550 °C.

**Table 2**

Vertical distribution of organic matter content (O.M%), Cation Exchange Capacity (C.E.C.) and exchangeable Ca, Mg, Na and K.

Location	Depth (cm)	O.M%	CEC cmol(c) kg <sup>-1</sup>	Exch Ca cmol+ kg <sup>-1</sup>	Exch Mg cmol+ kg <sup>-1</sup>	Exch Na cmol+ kg <sup>-1</sup>	Exch K cmol+ kg <sup>-1</sup>
Grassland	30	1.40	26.89				
	70	0.74	22.95				
	120	0.43	21.85				
A7	25	2.20	23.37	14.51	6.15	0.85	1.86
	85	0.55	20.91	3.17	4.81	10.94	1.99
	100	0.57	21.09	6.70	4.24	11.07	2.16
	120	0.38	20.35	4.86	5.17	8.88	2.01

**Table 3**

Relationship between the characteristic gravimetric water contents and clay matrix microstructural properties. Ws = shrinkage limit, AEP = Air Entry Point, Wp = plasticity limit, WI = liquidity limit, K = hydraulic conductivity, e = void ratio, n = porosity.

	W%	K m s <sup>-1</sup>	e	n
Ws	20	1.10 <sup>-11</sup>	0.5	0.34
AEP	27	2.10 <sup>-11</sup>	0.7	0.41
Wp	40	1.10 <sup>-10</sup>	1	0.51
WI	70	1.10 <sup>-5</sup>	1.8	0.64

layers) than deeper horizons, but the deeper layers have homogeneous texture and mineralogy (Tables 1–3; Righi et al., 1995; Bernard, 2006; Bernard et al., 2007; Bernard-Ubertosi et al., 2009; Dudoignon et al., 2007, 2009; Gallier et al., 2012;

- 0.4-to-2.4% weight organic matter,
- 20-to- 27 cmol(c) kg<sup>-1</sup> CEC according to the dominant illite content,
- and shrinkage (Ws), plasticity (Wp) and liquidity (WI) limits equal to 20%, 40% and 70% of gravimetric water contents, respectively.

The soils may be classified as Vertic Halaquept in the US soil taxonomic system and in Pelosol of the INRA pedologic referential (Baize and Girard, 1995; Pons and Gerbaud, 2005).

The main polder effect has been the descending of the groundwater table and progression of a desiccation front from the surface to the deeper layers. The surface illitisation phenomenon generally observed is limited to 20–30 cm depth according to the maturation of soil (Righi et al., 1995). Nevertheless, the effect of the surface illitisation induces only weak C.E.C. evolutions (Table 2). Furthermore, the eventual effect on the hydrodynamic behavior of the clay matrix is largely masked

by the surface structuration of soil in solid state for water contents between Wr and Wp. The resulting moisture profiles with soil depth show an increase in the gravimetric water content (W) from the Ws-Wp solid state in the surface layer to the Wp-Wl plastic state in the deep layers (Fig. 1a). The high shrinkage properties of the clay material have caused the spread of large shrinkage fractures from the surface to the depth at which the water content is equal to Wp (Bernard et al., 2007; Dudoignon et al., 2007). The meso and macro-cracks associated to shrinkage stop at the depth of Wp as the material becomes plastic, and, as the result, the clayey matrix is only characterized by microporosity between clay and silt particles (Dudoignon et al., 2007). The soil state nearby Wp induces a very low clay matrix hydraulic conductivity ( $K_s 10^{-10} \text{ m s}^{-1}$ ; Table 3). As a result, the surface 0-Wp layer's significant hydraulic conductivity is limited to the shrinkage crack network (about  $10^{-6} \text{ m s}^{-1}$  in the 0–50 cm layer). The macro-porosity of surface is particularly sensitive to weather conditions. The subjacent layer in which W varies between Wp and Wl is free from fracture. The hydraulic conductivities at saturation ( $K_s$ ) can increase with depth according to the clay matrix microstructure from  $10^{-10} \text{ m s}^{-1}$  to  $10^{-6} \text{ m s}^{-1}$  between the depths for which W is equal to Wp and Wl, respectively (Bernard, 2006; Gallier et al., 2012). The  $K_s$  of  $10^{-6} \text{ m s}^{-1}$  of the subjacent sub-liquid layer allows fresh water supply from the peripheral limestone into the subjacent reservoir. Thus, the desiccation mechanism of the primary fluvio-marine sediments and the development of different structures of the clay matrix with depth lead to the differentiation of two superimposed isolated reservoirs above and below the depth for which W=Wp. The fractured surface layer is leached by rainfall. The subjacent layer, initially saturated by salt water, shows a decrease in groundwater salinity from the inner part to the periphery of the basin (Weng et al., 2003; Gallier et al., 2012; Radimy et al., 2013, 2014).

In order to lower the depth at which W=Wp and to increase the thickness of desalinized soils for grain cropping, large surfaces of the territories have been progressively drained since the 1970's. Consequently, hydraulic management has progressively divided the territories into undrained fields for grassland and drained fields for grains. In the latter, the groundwater level is governed by drains placed 10 or 20 m apart buried at about 1 m deep. The Wp limit is attained at approximately 100 cm depth in these fields. On the contrary, in the grassland the groundwater level can stabilize at a depth of around 20 cm during the wet season and go down to 70–100 cm during the dry season. However, despite drainage, the territories always show characteristics of silty-to-clay shallow groundwater profiles.

The salinity profiles have been approached by looking at 1/5 Electrical conductivity ( $EC_{1/5}$ ) (Rhoades, 1982; Rayment and Higginson, 1992; Rhoades et al., 1990; Pons and Gerbaud, 2005). This measurement of the electrical conductivity of the electrolyte obtained by mixture of 10 g of dried soil in 50 g of distilled water characterizes a bulk ionic concentration of the electrolyte. Finally the salinity of ground water can be calculated level by level by taking into account the W of each sample (Montoroi, 1997). The measured  $EC_{1/5}$  profiles have clearly confirmed the fresh water inlet from the peripheral limestone into the subjacent reservoir (Fig. 1b). They have also demonstrated the surface desalinization caused by the deepening of groundwater levels. In spite of a general topography level close to 1–3 m above the sea level, the grassland areas are characterized by a typical microtopography resulting from the recurrent "mud cleaning" of the peripheral ditch. The extracted mud has been deposited along the ditch banks. This has led to a micro-topography and the development of mesophile to meso-hygrophile vegetation domains. In the drained fields the deepening of the groundwater level allowed the development of mesohygrophile to hygrophile domains (Radimy et al., 2013, 2014; Fig. 1b).

## 2.2. Methods

The AWC profiles were studied in an area of undrained grassland (L3) and in two drained cornfields (A7) in the INRA experimental site of St Laurent de la Prée (Rochefort, France). The two studied cornfields differ by drains placed 10 and 20 m apart: i.e. A7–10 m and A7–20 m respectively. The investigation sites were localized midway between two drains: i.e. 5 m or 10 m from the drains. They were equipped with piezometers for the recording of groundwater levels and eventual groundwater sampling. In fact, the analysis of the chemical composition of the sampled groundwater showed only average composition characteristics of fresh water and salt groundwater mixtures: i.e. fresh water near the surface and salt in depth. The  $EC_{1/5}$  and W profiles were measured on soils sampled every 10 cm from soil surface to a depth of 1.00 m using hand auger drills. The gravimetric water content (W) was calculated in reference to dried weight of samples after drying at 105 °C for at least 24 h. The data were periodically measured from June 11th to September 9th, 2013, according to weather changes and to the successive stages of plant growth since the output of the plant to the harvest (Fig. 4). Accurate vertical salinity gradients were obtained using the  $EC_{1/5}$  following two successive steps:

- The calculation of fluid conductivity ( $EC_f$ ) profiles from the coupling of  $EC_{1/5}$  and W profiles following the Montoroi formulae (Montoroi, 1997):

$$EC_f = EC_{1/5} W \quad (1)$$

with  $EC_f$ =the *in situ* fluid conductivity,  $EC_{1/5}$  the soil conductivity measured in laboratory and W the gravimetric water content.

The transformation of  $EC_f$  profiles to water salinity profiles in NaCl equivalent following abacus of resistivity – salinity relationship of fluid (Chapellier, 2001; Gallier, 2011). The conductivity – salinity may approximated as: eq. NaCl salinity (mg/L)=0.6  $CE_{1/5}$  ( $\mu\text{s}/\text{cm}$ ) in the 15 °C–20 °C domain.

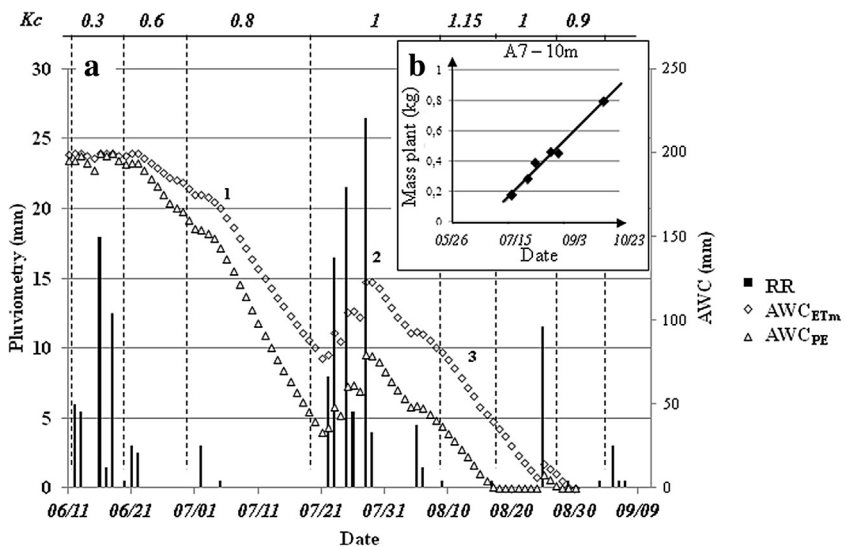


**Fig. 4.** a- The  $AWC_{PE}$  (white triangles) and  $AWC_{ETm}$  (white diamond shapes) evolutions from June to September 2013 have clearly shown the three successive periods: 1 = first desiccation, 2 = rehydration, 3 late and final desiccation. Corn  $K_c$  values in upper abscissa. Vertical black lines = rainfall. b- Average dry mass of plant measured from June to September.

The PE was calculated from an *in situ* weather station recording (temperature, wind direction and intensity, rainfall, sun radiation). The ETm for cornfields was calculated applying successive  $K_c$  to the PE (Fig. 3); i.e.

$$ETm = PEKc \quad (2)$$

with  $K_c$  according to the stages of the plant development.

The successive calculated Available Water Capacities were:

the “reference”  $AWC_{ref}$  calculated using the difference between the field capacity ( $W_{fc}$ ) and the wilting point ( $W_{wp}$ ) according to the soil texture (Mathieu and Pieltain, 1998; Baize, 2000; Rab et al., 2011): i.e.  $AWC_{ref} = h \times \gamma d (W_{fc} - W_{wp}) \times 10$ , with  $h$  being the thickness in m,  $\gamma d$  the dry bulk density of soil,  $W_{fc}$  and  $W_{wp}$  may be calculated taking into account the clay/silt ratio (Rawls et al., 1982). The “reference”  $AWC_{ref}$  may be also calculated directly via the texture triangle. The “reference”  $AWC_{ref}$  varies from 185 to 200 mm for the studied soil (Radimy et al., 2013).

- The  $AWC_{PE}$  is calculated using the difference between  $AWC_{ref}$  and the measured PE plus the rainfall (RR), as follows:

$$AWC_{PE} = AWC_{ref} - PE + RR \quad (3)$$

- The  $AWC_{ETm}$  calculated using the difference between  $AWC_{ref}$  and the calculated ETm, plus the rainfall (RR), as follows:

$$AWC_{ETm} = AWC_{ref} - ETm + RR \quad (4)$$

the “real” or “residual” PAW calculated for each day (D) and each depth (d) using the difference between the water contents  $W_{d/D}$  measured along the successive profiles and the reference  $W_{wp}$  (Radimy et al., 2013, 2014):

$$PAW = h \gamma d (W_{d/D} - W_{wp}) 10 \quad (5)$$

The  $W_{wp}$  is usually assessed as the equivalent 4.2 pF (15,000 hPa matric potential), thus around the shrinkage limit ( $W_s$ ) for clay dominated soils: i.e. around 25% for clayey soils and 19% for clay-silt (Mathieu and Pieltain, 1998; Bruand et al., 1996). For the following calculations, the  $W_{wp}$  was taken as equal to the  $W_s$  (20%) for the silty-clay soils of St Laurent de la Prée. The  $W_{fc}$  is equivalent to the 2.5 pF (330 hPa matric potential). It is mainly governed by the soil texture and  $W$  values varying in the  $W_s - W_p$  domain: that is, commonly, from 30% to 40% for clay dominated soils to silty clay soils (Mathieu and Pieltain, 1998; Nemes et al., 2011). The calculation of  $W_{fc}$  from a pF = 2.5 applied to our clay matrix gave a  $W_{fc}$  value of 40% equivalent to the  $W_p$  contents with an average bulk soil density of  $1.45 \text{ g/cm}^3$  (Bernard, 2006).

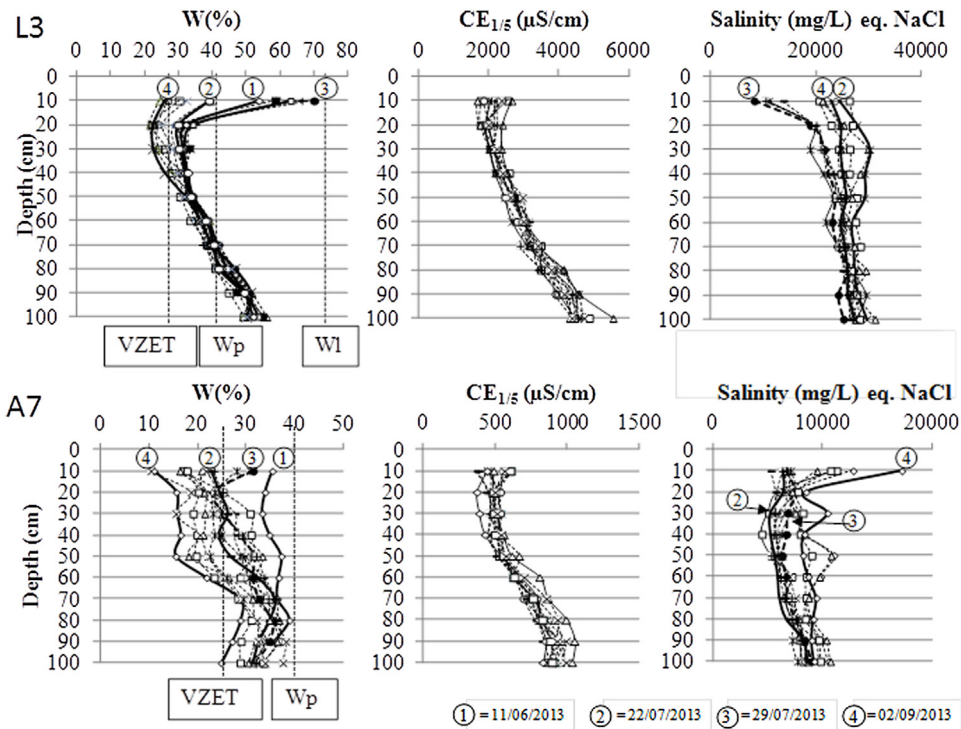


**Fig. 5.** Evolution of the L3 and A7–10 m water content profiles and associated  $EC_{1/5}$  and equivalent NaCl salinity profiles showing the impact of the three successive 06/11–07/22/2013 drying (1), 07/22–07/29 raining (2) and 07/29–08/23/2013 drying (3) periods. VZET = lower limit of unsaturated zone (vadose zone evapotranspiration).

### 3. Results

#### 3.1. Meteorological and PE/ET<sub>m</sub> data

In the following paragraphs, the presentation of the study results and the discussion are based on the three successive periods as follows: 1 the first desiccation (June 11–July 22), 2 the rainy period (July 22–July 29) and 3 the last desiccation (July 29–September 9).

The  $AWC_{PE}$  and  $AWC_{ETm}$  were calculated from June 11th to September 9th, 2013. They were representative of three successive periods (Fig. 4). The first period, from June 11th to July 20th, corresponded to a drying period and to the decrease of the AWC values. The slower decrease of the  $AWC_{ETm}$  was due to low corn Kc crop coefficients (0.3, 0.6 and 0.8) characteristic of the early growth of the corn. The first desiccation period was followed by a wet period associated with AWC increases resulting from rainfall during the period of July 20th to the 30th. The third period, beginning July 30th, corresponded to a final summer drying period. After July 30th the corn growth is maximum and its Kc is equivalent (1) to that of the grassland, thus the slopes of the  $AWC_{ETm}$  and  $AWC_{PE}$  are quite parallel.

#### 3.2. W profile behaviors

In the L3 the drying-wetting effect on the W profiles was limited to the 0–60 cm surface layer (Fig. 5). On the contrary, the W profiles remained quite superimposed for depths greater than 60 cm. The weather effect was stopped by the significant impermeability of the layer when W is equal to  $W_p$ , i.e. with the lowest macroporosity (Bernard, 2006; Bernard et al., 2007; Fig. 5). In the surface layer, the average W decrease was around 10%. The minimum reached by W was 22%, the W profile remained in the solid  $W_s$ - $W_p$  domain of the clay material. The rainy period induced an increase of W. It was limited to 10% in the 20–60 cm layer, but reached 70% in the 0–20 cm surface layer. This storage of rainwater in the 0–20 cm surface layer was caused by the  $W_p$  layer effect at the base of the surface layer (low permeability and end of the shrinkage fractures). It was accentuated by grass rooting, which has modified the soil structure of the surface layer by generating a micro-crack network and associated peds. The final drying period corresponded to the evapotranspiration of the surface and the regress of the W profiles to the dry state previously reached at the end of the first drying period (07/22/2013). The groundwater level was quite constant around 60–70 cm depth (i.e.  $W=W_p$ ) during the first drying period (Fig. 7). The drying effect was also limited to a depth of 50 cm because of the compactness of the unfractured  $W_p$  solid state of the clay matrix which limit the rooting in depth while allowing the capillary rise of salty water. It showed a drastic ascent during the rainy period of

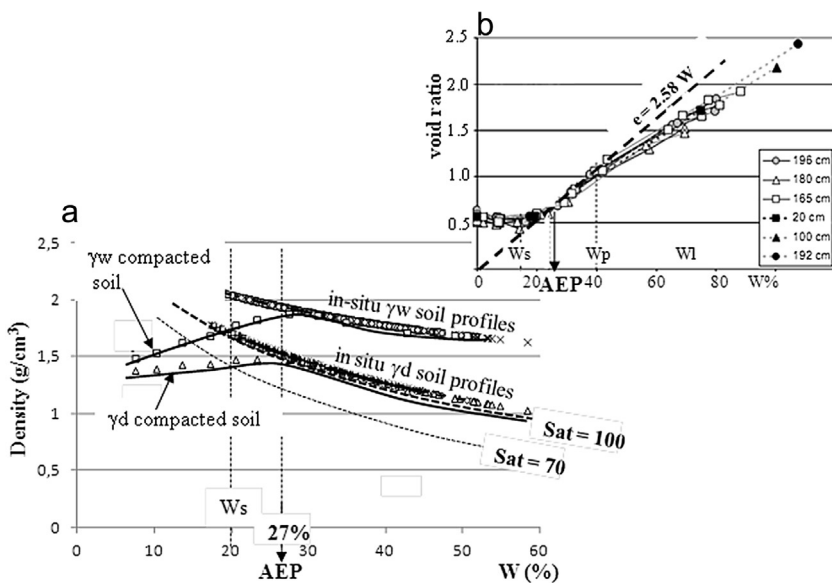


**Fig. 6.** a – Void ratio ( $e$ ) versus  $W$  diagram relationship between the water content profile and shrinkage curve of the clay matrix for different depths of sampling.b – Superimposition of the clay matrix shrinkage curve (in situ soil profiles) and soil compaction curve. White squares =  $\gamma_w$  (wet density), white triangles =  $\gamma_d$  (dry bulk density), Sat = saturation index, 100% and 70%.  $r_w$  = wet density,  $r_d$  = dry density, AEP = air entry point.

up to 30 cm, and a descent limited to 80 cm during the last drying period. As a consequence, the variations in groundwater level are quite limited to the surface layer with  $W$  comprised between  $W_s$  and  $W_p$ . This shows that water fluxes through the  $W_p$  layer are very weak and slow, associated to very high kinetics of desiccation – rehydration.

In the A7 field, the initial 06/11/2013  $W$  profile was quite constant around 35% (Fig. 5). The first desiccation event induced a shift of the  $W$  profile (07/22/2013) towards lower  $W$  values. The  $W$  decrease was significant at the surface but nearly zero at a depth of 60 cm. The  $W$  gradient was well developed from the surface down to the 60 cm depth, and corresponded to the vertical progression of the desiccation front. Near the surface (10 cm) the  $W$  fell below the  $W_s$  limit. The rainfall period weakly affected the  $W$  profile. In fact, only the 0–20 cm surface layer showed a significant  $W$  increase. In the 20 cm-to-100 cm layer,  $W$  profiles remained largely superimposed from July 22nd to the 29th. On the contrary, the final drying period caused a drastic  $W$  decrease all along the 0–100 cm  $W$  profile. Nevertheless, one can distinguish the 0–60 cm layer, characterized by large decreases of  $W$  below the  $W_s$  limit, from the 60–100 cm layer, characterized by a relatively weak shift of the  $W$  values (-15%) while remaining in the  $W_s$  –  $W_p$  domain. Simultaneously, and in spite of the rainfall period, the groundwater level showed a slow and continuous descent from 60 cm to 70 cm depth between June 11th and July 22nd. On the contrary, the last drying period led to a drastic descent of the groundwater level to a depth of 100 cm between July 29th and August 23rd (Fig. 5).

### 3.3. Air entry point calculation

As mentioned above, the structuring of the clay matrix with desiccation and shrinkage lead to the formation of a bimodal distribution of pore sizes: mesopores and macropores due to shrinkage cracks and clay matrix inter-particle micropores. The reference  $W_{fc}$  is commonly considered as the soil water content after drainage of gravity water. Regarding the very low hydraulic conductivity of the clay matrix in solid state ( $W_s$  –  $W_p$  domain), the field capacity has to be associated to the drainage of only the shrinkage cracks, while the clay matrix between the cracks is still saturated. One of the difficulties for the changing microstructure is to estimate the saturation index of the clay matrix constituting the inner part of peds and/or prisms. It was calculated by superimposition of the shrinkage curve of the clay matrix (Fig. 6a) on the compaction curve of the soil (Fig. 6b). The shrinkage curve was obtained step by step by progressive desiccation of small, intact cylindrical samples (Bernard, 2006; Bernard et al., 2007). The compaction curve was obtained following the Normal Proctor Test (norme N FP 44-093, 1999; Fig. 6). The water content equivalent to the Air Entry Point (AEP) in the clayey peds corresponds to the detachment of the shrinkage curve from the shrinkage line just before the shrinkage limit. It corresponds also to the detachment of the 100% saturation curve from the proctor dried density curve (Fig. 6b). It was estimated at  $W = 27\%$ . This AEP water content was used to locate the base of the vadose zone along the successive water profiles (Fig. 7). One can observe the role of drainage in smoothing the water table and vadose zone level, and, consequently, the potential change in groundwater recharge (Healy and Cook, 2002; Delin et al., 2007). The difference between the water table level and the depth of unsaturated zone determines the thickness of the groundwater-saturated zone (GWET). The evolution of the  $W = 27\%$  depth is quite parallel

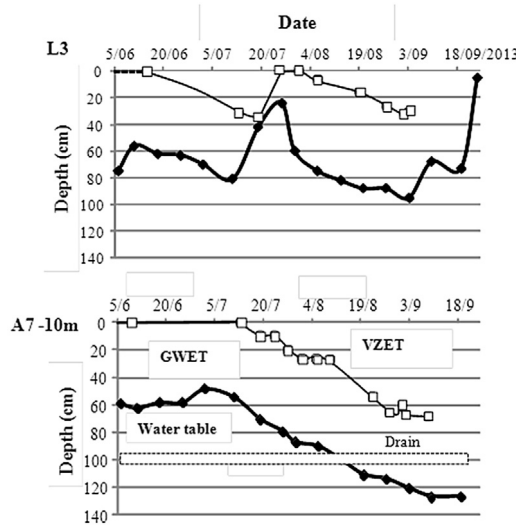


**Fig. 7.** Evolution of the water table level (black diamond shapes) and interface between the saturated groundwater (GWET) and vadose zone evapotranspiration (VZET; white squares) in L3 and A7-10m, from 05/06 to 18/09/2013. VZET = lower limit of unsaturated zone (vadose zone evapotranspiration). Black diamonds = water table level, white square = limit between GWET and VZET.

to the water table level. For a water table level inferior to 60 cm depth, the soil is saturated up to the surface. Thus, the thickness of the GWET is quite constant around 50–60 cm.

### 3.4. Representation of the AWC profiles

The AWC<sub>ref</sub>, AWC<sub>PE</sub> or AWC<sub>ETm</sub> were initially calculated according to the soil texture, or the W<sub>fc</sub> – W<sub>wp</sub> difference, eventually taking into account the PE or ET<sub>m</sub> and rainfall recordings. When multiplied by the depth, these AWC reference profiles allow the extrapolation of vertical AWC<sub>ref</sub>, AWC<sub>PE</sub> or AWC<sub>ETm</sub> profiles. Unfortunately, these AWC profiles are simple straight lines whose slopes are equivalent to the AWC<sub>ref</sub>, AWC<sub>PE</sub> or AWC<sub>ETm</sub> values (Fig. 8). In fact, the AWC<sub>PE</sub> and AWC<sub>ETm</sub> profiles are necessarily impacted by weather changes, by the water consumption of plants and their K<sub>c</sub>, and finally by the W profile evolutions.

In order to be the most realistic regarding the downward progression of the desiccation front, the calculation of the “real” or residual PAW was based on the successive W profiles. For each W profile the water contents (W<sub>d/D</sub>) were measured for successive dates (D) and different depths (d) in increments of 10 cm from the surface down to a depth of 100 cm. Consequently, the residual PAW<sub>s</sub> were calculated in increments of 10 cm following the equation:

$$\text{PAW} = h\gamma d(W_{d/D} - W_{wp}) \quad (6)$$

with h being the 10 cm thickness of each layer,  $\gamma d$  the dry soil bulk density, W<sub>d/D</sub> the gravimetric water content at d depth and D day, W<sub>wp</sub> the wilting point equivalent to the 20% W<sub>s</sub>.

The PAW profiles were calculated to the depth of n superimposed 10 cm layers, by summation of the PAW calculated for each 10 cm layer as follows:

$$\text{PAW}(n/D) = \sum_1^n h\gamma d(W_{i/D} - W_s)10 \quad (7)$$

with n being the number of 10 cm layers (that is to say n\*10 cm depth),  $\gamma d$  the soil bulk density, W<sub>i/D</sub> the gravimetric water content measured in the i layer at the D day, W<sub>s</sub> the shrinkage limit.

Under these conditions, the PAW profile behavior can be realistic according to surface conditions, the wilting point approach, the depth of rooting and the shallow groundwater level fluctuation (Radimy et al., 2013, 2014). This calculation of the PAW profiles based on the replacement of the W<sub>fc</sub> – W<sub>wp</sub> difference by W<sub>i/D</sub> – W<sub>s</sub> results in an evolution of the PAW profiles from the initial linear AWC<sub>PE</sub> or AWC<sub>ETm</sub> profiles to new profiles characterized by concave shapes representative of the successive D moisture profiles (Fig. 8).

### 3.5. L3 “Residual” PAW profiles

The first desiccation event provoked the downward progression of the desiccation front to the depth of 50 cm (Fig. 5). The consequence of this was the shift of the PAW profiles near the surface towards the AWC<sub>PE</sub> profiles. On the contrary, in deeper layers the PAW were unaffected by the desiccation, thus, the concave shapes of the PAW profiles were mainly enhanced by the surface desiccation (Figs. 5 and 8).

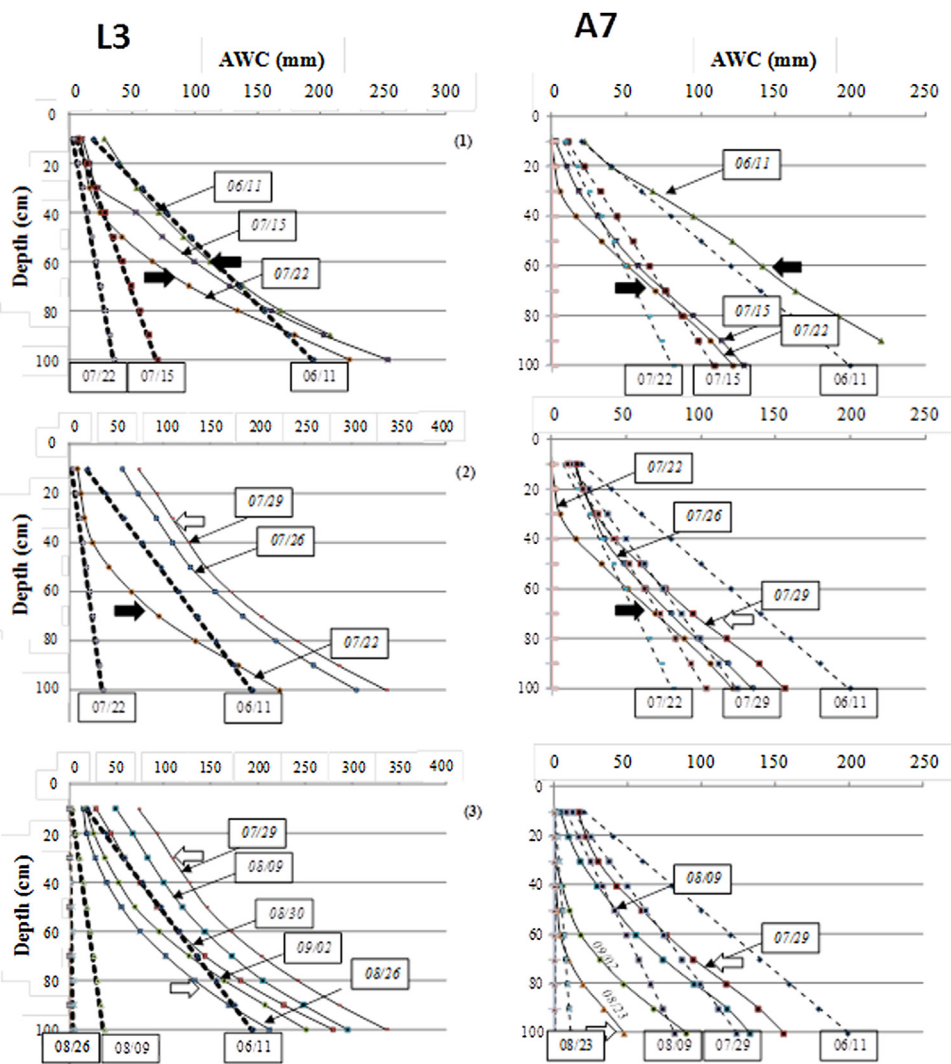


**Fig. 8.** Evolution of the “real” or residual PAW profiles in the L3 and A7 fields during the first desiccation (6/11, 07/15, 07/22/2013), rehydration (07/22, 07/26, 07/29/2013) and late desiccation (07/29, 08/09, 08/23, 09/02/2013) periods. Dotted lines =  $AWC_{PE}$  (L3) and  $AWC_{ETm}$  (A7) profiles, black line = PAW profiles. Large horizontal arrows = piezometric levels. Abcissa = AWC and PAW values in mm.

The rainy period (2), according to the increase of W contents in the surface layer, provoked the shift of the PAW profiles above the initial June 11th PAW profile (Figs. 5 and 8). In spite of the relatively unchanged W profile in deeper layers, the method of PAW calculation prompted the overall shift of the profiles.

Obviously, the last desiccation period provoked an inverse shift of the PAW profiles under the initial June 11th PAW profile. Nevertheless, and in spite of the descent of the groundwater level, the PAW profiles remain above the calculated  $AWC_{PE}$ . The calculations demonstrate the realism of the PAW profile representation when compared to the simple linear  $AWC_{PE}$  profiles. They correspond to the shallow impact of the grass rooting (30–40 cm deep). They also demonstrate the effect of rainwater storage in the surface layer caused by the low permeability of the intermediate W<sub>p</sub> layer.

### 3.6. A7 “Residual” PAW profiles

Despite a fairly constant groundwater level, the first desiccation event led to a drastic shift of the PAW profiles from the initial  $AWC_{ref}$  below the  $AWC_{ETm}$  profiles in the 0–60 cm surface layer. The surface effect of the desiccation is also clearly shown by the concave shape of the profiles near the surface (Figs. 5 and 8).

The rain event (2) provoked the overall shift of the PAW profiles from July 22nd toward the successive  $AWC_{ETm}$ .

The last desiccation event (3) led to the decrease of the water contents below the shrinkage limit W<sub>s</sub> from the surface to a depth of 60 cm. The consequence of this is the progressive shift of the PAW profiles toward near zero in this surface

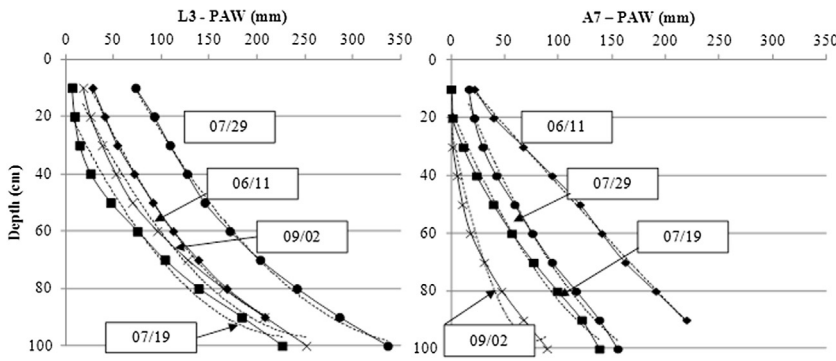


**Fig. 9.** Representative depth/PAW profiles in L3 and A7 calculated for 06/11, 07/19, 07/29 and 09/02/2013. Black lines = calculated PAW from the W profile. Dotted line = associated second-degree equations (Table 1).

layer. The deepening of this “zero PAW” surface layer clearly shows the downward progression of the water stress and the necessity of the root network to reach the water-rich deep layers (Fig. 8).

### 3.7. Equations of depth/PAW profiles

According to the measured W profiles and to Eq. (7), the PAW profiles are represented in depth versus PAW diagrams: i.e. PAW as abscissa (Fig. 9). In the undrained grassland, the PAW profiles vary according to the depth to show concave curve patterns. The concavity is mainly caused by the surface desiccation front. In the drained field, the PAW profiles vary according to the depth to show double curve patterns: i.e. a concave curve near the surface, caused by the downward progression of the desiccation front, and a significantly convex curve in depth according to the drain efficiency and capillary rise (Figs. 8 and 9). The calculated PAW profiles are mainly governed by the W profiles, according to the weather conditions and water consumption of plants, and by the groundwater level and associated capillary fringe.

A first step is to propose the numerical equations for the representation of the PAW profiles in the depth versus PAW diagrams, to a depth of at least 100 cm. A second step is to propose the modeling of the PAW profiles in the inverse PAW/depth representation. The model has to be based on an easily measurable surface parameter.

The successive depth/PAW profile equations were attempted with basic functions: exponential, logarithmic, power law, and 2nd degree polynomial. The exponential equations give only convex depth/PAW patterns, unrealistic relative to real PAW profiles. The logarithmic depth/PAW calculated profiles are superimposed on the grassland PAW profiles ( $R^2 = 0.99$ ), but impossible to superimpose on the PAW profiles in the drained fields ( $0.68 < R^2 < 0.90$ ). Moreover, the surface decrease of the W near Ws leads to associated PAW=0, which is inconsistent with the logarithm function. The Power law allows the concave PAW patterns. Nevertheless, they are weak when superimposed onto the real profiles, with  $R^2$  correlation coefficients decreasing to 0.91 in grassland and 0.73 in drained parcels. The PAW=0 in the surface layer also provokes an inconsistency of calculation.

The 2nd degree depth/PAW profiles are calculated as following:

$$\text{depth} = A(\text{PAW})^2 + B\text{PAW} + C \quad (8)$$

The calculated profiles are superimposed onto the measured profiles. Despite small shifts observed near a depth of 1.00 m for the driest profiles, they show realistic patterns (Fig. 9; Table 4). The A decrease enhances the curve concavity, the B decrease provokes the increase of the initial surface slope and the C increase provokes the global shift of the curve with respect to  $\text{PAW} \geq 0$  (Fig. 10).

### 3.8. PAW/Depth profile modeling

According to the realistic representations of the calculated *depth/PAW* (Eq. (8)), the modeling of the PAW/depth profiles was also attempted using a second degree polynomial equation as follows:

$$\text{PAW} = A'\text{depth}^2 + B'\text{depth} + C' \quad (9)$$

with  $A'$ ,  $B'$  and  $C'$  the new parameters to determine.

The simple axis transposition allowed very accurate  $R^2$  correlation coefficients, which are grouped between 0.99 and 1.0 in the grassland and between 0.98 and 1.0 in the drained field (Table 4). The  $A'$ ,  $B'$  and  $C'$  parameters act as  $A$ ,  $B$ ,  $C$  in the initial “ $\text{depth} = A(\text{PAW})^2 + B\text{PAW} + C$ ” profiles.  $A'$  governs the concavity of the profiles in depth.  $B'$  governs the concavity of the profiles up to the surface.  $C'$  provokes the whole shift of the profiles, but  $C'$  is positive in this second equation.

The third step is to determine eventual realistic relationships able to link  $A'$ ,  $B'$ , and  $C'$  with a physical parameter which may be easily measurable from the surface. These are PE or ET<sub>m</sub>, the rainfall (RR), or the AWC<sub>ref</sub> calculated by the weather station,

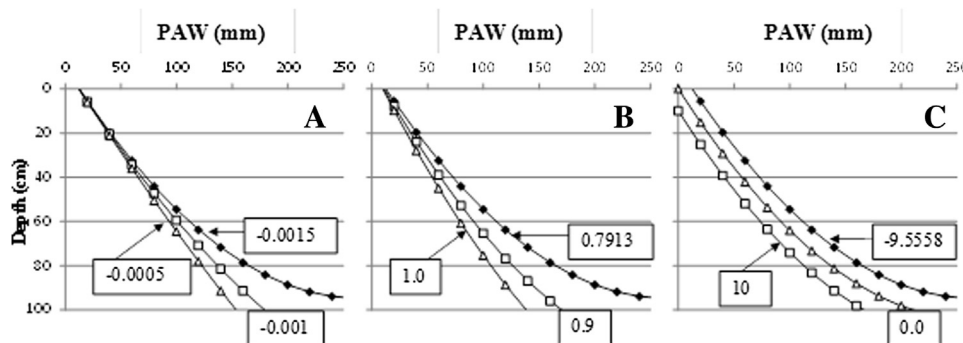
**Table 4**

Evolution of the A, B, C and A', B', C' parameters of the  $\text{depth} = A(\text{PAW})^2 + B(\text{PAW}) + C$ , and  $\text{PAW} = A'\text{depth}^2 + B'\text{depth} + C'$  profile equations in L3 grassland and A7 drained field.  $R^2$  = correlation coefficients.

Grassland (L3)				PAW = f(Depth)				
Date	A	B	C	$R^2$	A'	B'	C'	$R^2$
6/11/2013	-0.0015	0.791	-9.55	0.99	0.0172	0.47	23.30	0.99
7/22/2013	-0.0018	0.756	14.78	0.96	0.0315	-1.08	18.51	0.99
7/29/2013	-0.0009	0.720	-36.97	0.99	0.0230	0.29	74.09	0.99
9/2/2013	-0.0013	0.703	3.38	0.98	0.0259	-0.26	19.97	0.99

Drained Field (A7)				PAW = f(Depth)				
Date	A	B	C	$R^2$	A'	B'	C'	$R^2$
6/11/2013	-9.00E-05	0.426	1.67	0.99	0.0015	2.32	3.49	0.99
7/22/2013	-0.0014	0.787	13.71	0.99	0.0097	0.38	-9.40	0.99
7/29/2013	-0.0021	0.951	0.19	0.99	0.0097	0.54	7.19	0.99
9/2/2013	-0.0096	1.629	28.37	0.96	0.0153	-0.72	8.02	0.99



**Fig. 10.** Schematic representation of the impact of the A, B and C parameters on the PAW profile patterns. The calculations are based on the 06/11/2013 PAW profile equation (black diamond shape). a-A = -0.0015, -0.001, -0.0005; b – B = 0.79, 0.90, 1.00; c-C = -9.6, 0.0, 10.0.

**Table 5**

Recapitulative table of attempts at  $A'$ ,  $B'$ ,  $C' - W_{10}$  and  $A'-B'$  linear relationships.

Grassland		Drained field	
Equation	$R^2$	Equation	$R^2$
$A' = f(W_{10})$	0.44	$A' = f(W_{10})$	0.15
$B' = f(W_{10})$	0.89	$B' = f(W_{10})$	0.61
$C' = f(W_{10})$	0.96	$C' = f(W_{10})$	0.11
$B' = f(A')$	0.89	$B' = f(A')$	0.17

the surface water content, and the groundwater levels. In the grassland and drained field, despite their clear relationships with the 3 successive periods these parameters showed only very weak relationships with  $A'$ ,  $B'$  or  $C'$ . Finally, according to the merits of the PAW profile calculation based on the W profiles, the PAW profile modeling was tested using the water content measured at the depths of 10 and 20 cm ( $W_{10}$  and  $W_{20}$  respectively).

In the grassland, periods 1, 2 and 3 led to a large range of  $W_{10}$  (Fig. 11). Despite the low  $R^2$  of 0.44 obtained for the  $A' - W_{10}$  linear relationship, the  $A'-B'$  and  $C'-W_{10}$  relationships are realistic (Figs. 11 and 12; Table 5). The accurate  $C'-W_{10}$  relationship corresponds to the role of the  $C'$  parameter on the horizontal shift of the PAW profiles associated with the desiccation and rainfall events (Fig. 11). The PAW profiles have been modeled by the second-degree polynomial equation (Eq. (9)), with  $A'$ ,  $B'$  and  $C'$  parameters determined from  $A'-W_{10}$ ,  $B'-W_{10}$  and  $C'-W_{10}$  linear relationship (Table 5). They are superimposed on the PAW profiles calculated from the W profiles (Eq. (7); Figs. 12 and 13).

In the drained field, the same  $A'$ ,  $B'$ ,  $C' - W_{10}$  diagrams corroborate the drainage impact by the very narrow 10–35%  $W_{10}$  domain. The first consequence is an  $A'$  parameter restricted to a very small domain, largely shifted from the  $A'$  domain of grassland. The second consequence, regarding the relative dispersion of the values, is the impossibility of obtaining a realistic  $A'-W_{10}$  relationship but only an average  $A'$  value at 0.01.  $B'$  increases as the  $W_{10}$  values (Fig. 11). A linear relationship may be established between  $B'$  and  $W_{10}$ , but with a low  $R^2$  coefficient of 0.61 (Table 5). According to the narrow domains of values, the  $C'-W_{10}$  couples are localized on the base of the linear  $C'-W_{10}$  domain characteristic of the grassland. In fact, calculating the relationship between  $C'$  and  $W_{10}$  also results in only an average value of  $C'$  restrained to 0–3. Nevertheless, these  $A'$  and

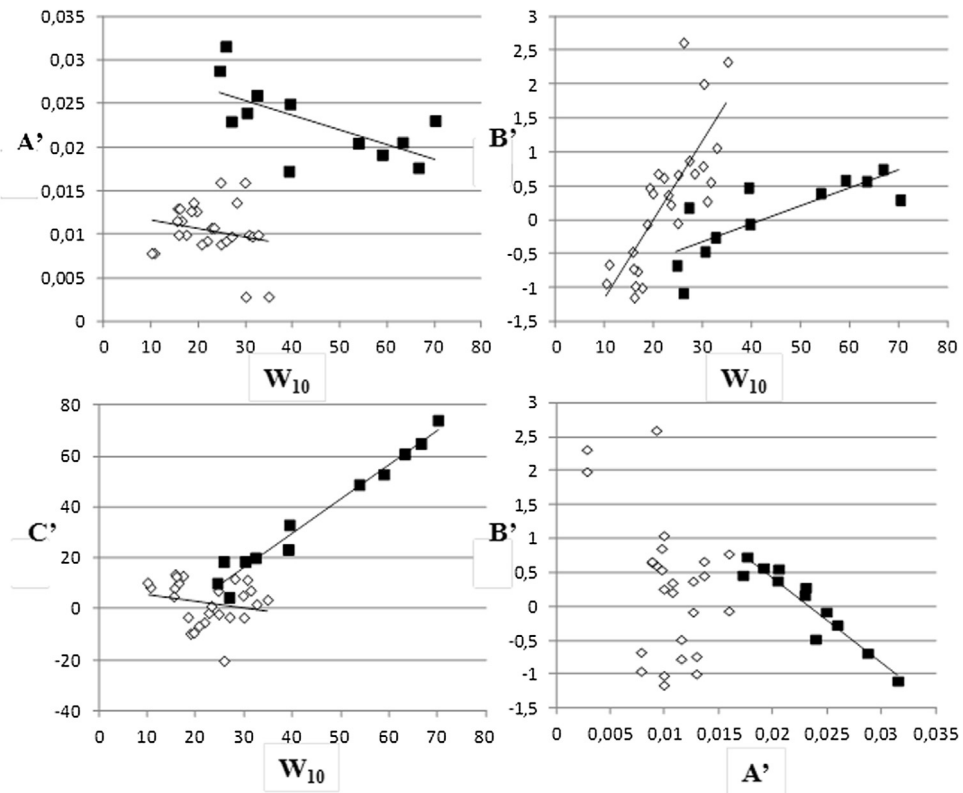


**Fig. 11.** A', B' and C'/W<sub>10</sub> and B'A' diagrams. Black squares = L3 grassland, white diamond shapes = A7 drained field. The straight lines are the best-calculated linear relations (Table 5).

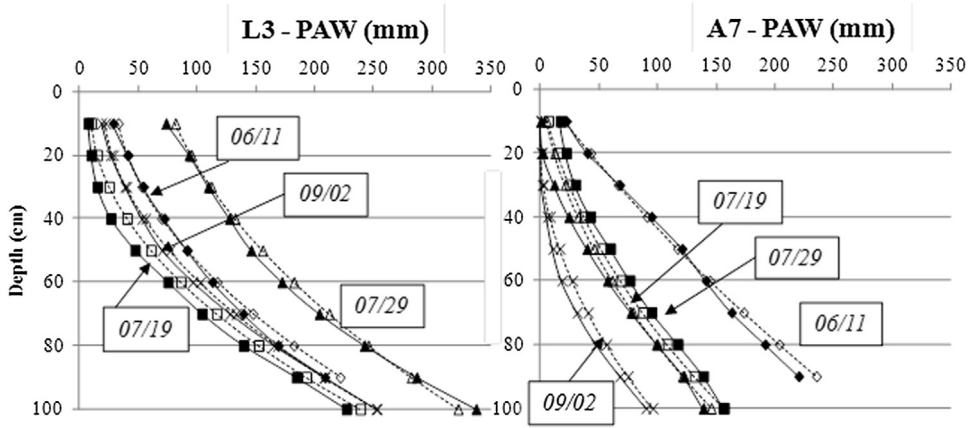


**Fig. 12.** Superimposition of the W<sub>10</sub>-modeled PAW profiles (dotted lines) on the W<sub>iD</sub>-calculated PAW profiles (black lines; Eq. (7)) for 06/11, 07/19, 07/29 and 09/02/2013.

C' average values may be slightly better defined using the calculated linear relationship despite the poor R<sup>2</sup> coefficients. The B' parameter is evaluated through the B'-W<sub>10</sub> relationship. Despite small differences observed on the driest profiles, the modeled PAW profiles are significantly superimposed on the PAW profiles calculated from the W profiles (Fig. 12). The comparison of the modeled and calculated PAW profiles, in a W-calculated PAW versus W<sub>10</sub>-modeled PAW diagram, shows also a strong relationship along the 1/1 straight line for all profiles measured during 2013: i.e. R<sup>2</sup> = 0.99 in L3 and R<sup>2</sup> = 0.94 in A7. The attempts at PAW modeling using the W<sub>20</sub> values provide similar results; significantly superimposed W<sub>n</sub>-calculated and W<sub>10</sub>-modeled profiles and R<sup>2</sup> coefficients superior to 0.98, indicative of the most realistic equations.

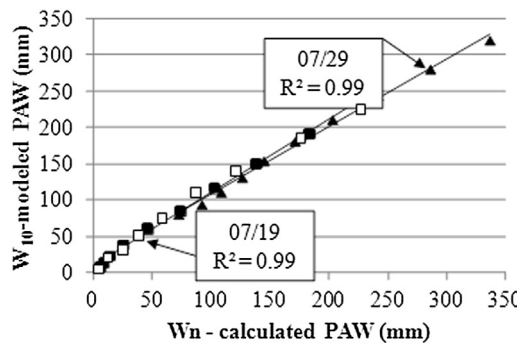


**Fig. 13.** The W-calculated PAW profiles and W<sub>10</sub>-modeled PAW profiles show 1/1 linear relationships with R<sup>2</sup> higher than 0.99, example of the 07/19 (black squares) and 07/29/2013 (black triangles). White square = example of W<sub>20</sub>-calculated profile (07/19).

#### 4. Discussion – conclusion

The coastal wetland territories were generally reclaimed from the sea by progressive desiccation of primary fluvio-marine sediments. The primary clay-dominated material was initially saturated by seawater. Nevertheless, along the basin periphery the salt groundwater may be mixed with fresh water of continental origin (Weng et al., 2003; Bernard, 2006; Gallier, 2011; Gallier et al., 2012). The phenomena of desiccation and surface leaching by rainfall plus the mixture of local seawater with fresh water have led to the formation of different salinity profiles that directly influence the farming methods and grain yields. These are the typical characteristics of a shallow salt groundwater that need to be controlled by drainage regarding the balance between capillary upflow and drainage below the root zone (Ayars et al., 2006a,b). Previous geophysical investigations by electrical methods have allowed the calibration of the Archie's law for this mineralogical homogeneous medium (Bernard, 2006; Bernard-Ubertosi et al., 2009). The parameters taken into account in the Archie's law are the porosity, saturation index of the medium and salinity (resistivity) of the water. Thus, the coupling of W profiles and resistivity profiles allows the extrapolation of salinity profiles (Gallier, 2011; Gallier et al., 2012). The method is particularly efficient to visualize the freshwater inputs in the periphery of the basin. The in situ measured resistivity sections allow the modeling of soil-to-sediment transition and associated salinity profile through the investigated fields. Nevertheless, the salinity profiles may be absolutely quantified using simple EC<sub>1/5</sub> profile measurements. They are used to characterize the different territories. Historically, the first stages of reclamation maintained the groundwater near the surface and conditioned the territories for grassland and cow breeding only. Since the 1970s, the intensive development of grain crops (corn) required the wide development of drainage, causing a deepening of groundwater level and associated soil desalinization.

In these shallow groundwater marshlands, a short study of the state pathways of the clay material constituting the soil allows us to determine the water content equivalent to the limit between the groundwater saturated soil and the vadose zone. In the undrained grassland, the VZET fluctuates between 0 and 40 cm depth only, according to the water table level evolution. In the drained grain field, the soil stays saturated until mid-July. The desaturation front drops under the surface from mid-July to September. It goes down parallel to the water table descending. The thickness of the vadose zone reaches its maximum of 70 cm in September. In this shallow groundwater, the capillary rise clearly governs the water content profiles, and consequently the associated PAW profile. Consequently, the different hydraulic managements act directly on both water and salinity profiles, so they govern the soil potential for the pedodiversity and crop yields. This paper demonstrates that the monitoring of the successive moisture profiles coupled with a simple study of the state pathways of the clay matrix along its shrinkage curve allows the monitoring of the VZET thickness.

Many authors have worked on and modeled water flow in the field using pedotransfer functions and consequently the PAW (Guber et al., 2009; Nosetto et al., 2009; Bruand et al., 2002, 2004; Burns, 1974; Cazemier et al., 2001; Nyvall, 2002). The difficulties are essentially the heterogeneity and complexity of the unsaturated media. Vertical AWC<sub>ref</sub> profiles and their seasonal behaviors may be also calculated from profiles of tensiometric pressures (Breda et al., 2002; Granier et al., 1995; Tardieu et al., 1990). Unfortunately, our clay-dominated soils are extremely sensitive to the shrinkage phenomenon. The drying effect provokes the deepening of a shrinkage crack network, which can make the tensiometer ineffective by early disconnection of the porous plugs (Radimy et al., 2013).

This paper proposes a methodology of calculation and modeling of the real or residual available water capacity « PAW » profiles in such clay dominated soils. This method is able to represent the PAW behavior caused by weather conditions and the water consumption of plants according to their rooting depth. Calibrated on the W profiles, it has been shown realistic to the depth of 1.00 m for undrained grasslands and drained grain fields. The PAW profiles can be easily calculated as a second-degree polynomial equation with respect to R<sup>2</sup> > 0.98. Even if the surface PE/ETm and/or AWC<sub>ref</sub> do not allow realistic relationships for the modeling of PAW profiles, the W<sub>10</sub> or W<sub>20</sub>, easily measurable in the surface layer, are satisfactory for PAW profile modeling in undrained grassland and drained fields. This methodology, coupled with the salinity profiles calculated from the W and EC<sub>1/5</sub>, may be used for the quantification and prediction of the water and salt stress in these wetland territories; thus, it can be used as a realistic tool for hydraulic management and farming in this region.

no conflict of interest

## Acknowledgements

The authors wish to thank the Regional Council of Poitou-Charentes and the firm of ERM for providing the funding for this research during the period of 2011 to 2014.

## Appendix A. Supplementary data

Supplementary data associated with this article can be found, in the online version, at <http://dx.doi.org/10.1016/j.jehr.2016.11.002>.

## References

- Archer, J.R., Smith, P.D., 1972. The relation between bulk density, Available Water Capacity: and air capacity of soils. *J. Soil Sci.* 23 (4), 475–480.
- Ayers, J.E., Schoneman, R.A., Dale, F., Meso, B., Shouse, P., 2001. Managing subsurface drip irrigation in the presence of shallow groundwater. *Agric. Water Manage.* 47, 243–267.
- Ayers, J.E., Christen, E.W., Hornbuckle, J.W., 2006a. Controlled drainage for improved water management in arid regions irrigated agriculture. *Agric. Water Manage.* 86, 128–139.
- Ayers, J.E., Christen, E.W., Soppe, R.W., 2006b. The resource potential of in-situ shallow groundwater use in irrigated agriculture: a review. *Irrig. Sci.* 24, 147–160.
- Baize, D., 2002. Guide of analyzes in pedology (In French), 2nd ed. INRA, 257 p.
- Baize, D., Girard, M.C., 1995. Référentiel Pédologique, Pedological referential (In French). INRA ed. 375 p.
- Bastet, G., Bruand, A., Quétin, P., Cousin, I., 1998. Estimating of water retention properties of soils using pedotransfer functions (PFT): A literature review. (In French, with English abstract). *Étude et Gestion des Sols* 5 (1), 7–28.
- Bates, J.M., Granger, C.W.J., 1969. The combination of forecasts. *Oper. Res. Q.* 20, 451–468.
- Bernard, M., Dudoignon, P., Pons, Y., Chevallier, C., Boulay, L., 2007. Structural characteristics of clay-dominant soils of a marsh and paleosol in a crossed diagram. *Eur. J. Soil Sci.* 58 (5), 1115–1126.
- Bernard, M., 2006. Study of the Behavior of Marsh Soils: Mineralogical, Structural and Hydromechanical Evolution. (Marshes of Rochefort and Marais Poitevin) (In French, with English Abstract) PhD Thesis. University of Poitiers, pp. 309.
- Bernard-Ubertosi, M., Dudoignon, P., Pons, Y., 2009. Characterization of structural profiles in clay-rich marsh soils by cone resistance and resistivity measurement. *Soil Sci. Soc. Am. J.* 73 (1), 46–54.
- Braudeau, E., Sene, M., Mohtar, R.H., 2005. Hydrostructural characteristics of two African tropical soils. *Eur. J. Soil Sci.* 56 (June), 375–388. <http://dx.doi.org/10.1111/j.1365-2389.2004.00679.x>
- Breda, N., Lefevre, Y., Badeau, V., 2002. Water reservoir of temperate soils: specificity and evaluation challenges. (In French, with English abstract). *La Houille Blanche, Revue Internationale de l'Eau*, 24–32.
- Bruand, A., Coquet, Y., 2005. Soils and water cycle (In french). Science du Sol et Environnement, Dunod, 345–363.
- Bruand, A., Duval, O., Gaillard, H., Darthout, R., Jamagne, M., 1996. Variability of soil water retention properties: importance of the bulk density (In French, with English abstract). *Etude et Gestion des Sols* 3 (1), 27–40.
- Bruand, A., Perez Fernandez, P., Duval, O., Quétin, Ph., Nicoulaud, B., Gaillard, H., 2002. Estimation of soil water retention properties: use of pedotransfer classes after textural and textro-structural stratification (In French, with English abstract). *Etude et Gestion des Sols* 9, 105–125.
- Bruand, A., Duval, O., Cousin, I., 2004. Estimation of soil water retention properties from SOLHYDRO database: a first proposal with type of horizon, texture and bulk density. (In French, with English abstract). *Etude et Gestion des Sols* 11, 323–334.
- Burns, I.G., 1974. A model for predicting the redistribution of salts applied to fallow soils after excess rainfall or evaporation. *J. Soil Sci.* 25 (2), 165–178.
- Carminati, A., Vetterlein, D., Weller, U., Vogel, H.J., Oswald, S.E., 2009. When roots lose contact. *Vadose Zone J.* 8, 805–809. <http://dx.doi.org/10.2136/vzj2008.0147>
- Cazemier, D.R., Lagacherie, P., Martin-Clouaire, R., 2001. A possibility theory approach for estimating available water capacity from imprecise information contained in soil databases. *Geoderma* 103, 113–132.
- Chapellier, D., 2001. Prospection électrique de surface, Cours online de géophysique, Electrical prospection, online course of geophysics University of Lausanne. Institut Français du Pétrole, 102 p.
- Choisnel, E., 1992. Calculation of the hydric balance: modeling options and complexity levels. (In French, with English abstract). *Scie. du sol.* 30 (1), 15–31.
- Couvreur, V., Vanderborght, J., Draye, X., Javaux, M., 2014. Dynamic aspects of soil water availability for isohydric plants: focus on root hydraulic resistances. *Water Resour. Res.* 50. <http://dx.doi.org/10.1002/2014WR015608>
- Delin, G.N., Healy, R.W., Lorenz, D.L., Nimmo, J.R., 2007. Comparison of local-to-regional scale estimates of ground-water recharge in Minnesota. *USA. J. Hydrol.* 334 (1), 231–249.
- Dudoignon, P., Causseque, S., Bernard, M., Hallaire, V., Pons, Y., 2007. Vertical porosity profile of a clay-rich marsh soil. *Catena* 70 (3), 480–492.
- Dudoignon, P., Bernard-Ubertosi, M., Hillaireau, J.M., 2009. Grasslands and coastal marshes management: role of soil structure. In: Hans Schröder, G. (Ed.), *Grasslands, Ecology, Management and Restore*. Nova Science Publishers, NY.
- Fan, J., Oestergaard, K.T., Guyot, A., Lockington, D.A., 2014. Estimating groundwater recharge and evapotranspiration from water table fluctuations under there vegetation covers in a coastal sandy aquifer of subtropical Australia. *J. Hydrol.* 519, 1120–1129.
- Gallier, J., Dudoignon, P., Hillaireau, J.M., 2012. Microstructure – hydromechanical property relationship in clay dominant soils. In: Aydinalp, Cumbur (Ed.), *In An Introduction to the Study of Mineralogy*. INTECH open access publisher, pp. 51–72.
- Gallier, J., 2011. Characterization of Structural Evolution Process and Salinity of Coastal Marsh Soil by in Situ Mechanical Measurements and Geo-electrical Investigations (In French) PhD Thesis. University of Poitiers, 218 p.
- Granier, A., Badeau, V., Breda, N., 1995. Water balance modeling of forest settlements (In French). *Rev. For. Fr. XLVN*, 59–68.
- Guher, A.K., Pachepsky, Y.A., Van Genuchten, M.T.H., Simunek, J., Jacques, D., Nemes, A., Nicholson, T.J., Cady, R.E., 2009. Multimodel simulation of water flow in a field soil using pedotransfer functions. *Vadose Zone J.* 8 (February (1)), 10p.
- Healy, R., Cook, P., 2002. Using groundwater levels to estimate recharge. *Ydrogeol. J.* 10, 91–109.
- Hong, S.Y., Minasny, B., Han, K.H., Kim, Y., Lu, K., 2013. Predicting and mapping soil available water capacity in Korea. *Peer J.* 1, <http://dx.doi.org/10.7717/peerj.71>, e 71. 20p.
- Javaux, M., Couvreur, V., Vanderborght, J., Vereecken, H., 2013. Root water uptake: from 3D biophysical processes to macroscopic modeling approaches. *Vadose Zone J.* 12, 1–16. <http://dx.doi.org/10.2136/vzj2013.02.0042>
- Kern, J.S., 1995a. Geographic patterns of soil water-holding capacity in the contiguous United States. *Soil Sci. Soc. Am. J.* 59, 1126–1133. <http://dx.doi.org/10.2136/sssaj1995.03615995005900040026x>
- Kern, J.S., 1995b. Evaluation of soil water retention models based on basic soil physical properties. *Soil Sci. Soc. Am. J.* 59, 1134–1141.

- Mathieu, C., Pieltain, F., 1998. Physical analysis of soil, Selected Methods (In French). Lavoisier TEC & DOC, PARIS ed. 275 p. France.
- Montoroi, J.P., 1997. Electrical conductivity of the soil solution and aqueous extracts – Application to a sulfated acid salty soil of Bassa Casamance – Senegal (In French, with English abstract). Etude et Gestion des sols 4, 279–298.
- Morvan, X., Bruand, A., Cousin, I., Roque, J., Baran, N., Mouvet, Ch., 2004. Predicting water retention properties of soils in a watershed using pedotransfer functions: influence of bulk density and coarse element content. (In French, with English abstract). Étude et Gestion des Sols 11 (2), 81–99.
- Nemes, A., Pachepsky, Y.A., Timlin, D.J., 2011. Toward improving global estimates of field soil water capacity. Soil Sci. Soc. Am. J. 75, 807–812, <http://dx.doi.org/10.2136/sssaj2010.0251>.
- Norme NF P 44-093, 1999. Characterization of References for Materials: Normal Proctor Test – Modified Proctor Test (In French). Recueil AFNOR Normes Géotechniques.
- Nosetto, M.D., Jobbàgy, E.G., Jackson, R.B., Sznajder, G.A., 2009. Reciprocal influence of crops and shallow groundwater in sandy landscape of the Inland Pampas. Field Crops Res. 113, 138–148.
- Nyvall, J., 2002. Soil Water Storage Capacity and Available Soil Moisture Resource Management Branch. Ministry of Agriculture, Food and Fisheries, Order No. 619000-1 4 p.
- Pons, Y., Gerbaud, A., 2005. Agricultural Classification of marsh soils based on the relationship between Sodicity and structural stability. Application to the case of the west marshes of France (In French, with English abstract). Etude et gestion des sols 12 (3), 229–244.
- Pons, Y., Capillon, A., Cheverry, C., 2000. Water movement and stability of profiles in drained, clayey and swelling soils: at saturation, the structural stability determines the profile porosity. Eur. J. Agron. 12, 269–279.
- Rab, M.A., Chandra, S., Fisher, P.D., Robinson, N.J., Kitching, M., Aumann, C.D., Imhof, M., 2011. Modeling and prediction of soil water contents at field capacity and permanent wilting point of dry land cropping soils. Soil Research 49(5): 389–407 <http://dx.doi.org/10.1071/SR10160>.
- Radimy, R.T., Dudoignon, P., Hillaireau, J.M., Debouté, E., 2013. Polder effects on sediment-to-soil conversion: water table, residual available water capacity, and salt stress interdependence. Sci. World J. 2013, <http://dx.doi.org/10.1155/2013/451710>, Article ID 451710, 20p.
- Radimy, R.T., Dudoignon, P., Hillaireau, J.M., Caner, L., 2014. Evapotranspiration – soil structure relationship in west marshes of France. J. Water Res. Prot. 6, 821–840, <http://dx.doi.org/10.4236/jwarp.2014.69078>.
- Rawls, W., Brakensiek, D., Saxton, K.E., 1982. Estimating soil water retention from soil properties. J. Irrig. Drain. Eng. 108 (IR2), 166–171.
- Rayment, G.E., Higginson, F.R., 1992. Australian Laboratory Handbook of Soil and Water Chemical Methods, Melbourne, Inkara Press. Australian Soil and Land Survey Handbooks, v.3.
- Rhoades, J.D., Shouse, P.J., Alves, W.J., Manteghi, N.A., Lesch, S.M., 1990. Determining soil salinity from soil electrical conductivity using different models and estimates. Soil Sci. Soc. Am. J. 54 (1), 46–54.
- Rhoades, J. D., 1982. Soluble Salts. In: A.L. Page (ed.) Methods of soil analysis, Part 2 Chemical and microbiological properties, 2nd ed. Agronomy 9: 149–157.
- Righi, D., Velde, B., Meunier, A., 1995. Clay stability in clay-dominated soil systems. Clay Miner. 30 (1), 45–54.
- Saxton, K.E., Rawl, W.J., 2006. Soil water characteristic estimates by texture and organic matter for hydrologic solutions. Soil Sci. Soc. Am. J. 70, 1569–1578, <http://dx.doi.org/10.2136/sssaj2005.0117>.
- Shah, N., Nachabe, M., Ross, M., 2007. Extinction depth and evapotranspiration from ground water under selected land covers. Ground Water 45 (3), 329–338.
- Tardieu, F., Katerji, N., Béthenod, O., Hamard, P., Quétin, P., Bal, P., 1990. Relations between the hydric state of soil, the basis potential and other indicators of water stress in maize (In French). Agron. EDP Sci. 1990 10 (8), 617–626.
- Tournade, F., Bouzillé, J.B., 1991. Relations between soil and vegetation in wet natural grasslands of the Marais Poitevin. Demonstration of an organizational model (In French, with English abstract). Soil Sci. 29 (4), 339–357.
- Tournade, F., Bouzillé, J.B., 1995. Soil determinism of plant diversity of ecosystems in grasslands of the Marais Poitevin: application to the definition of an agri-environmental management (In French, with English abstract). Etude et Gestion des Sols 2 (1), 57–72.
- Weng, P., Giraud, F., Fleury, P., Chevallier, C., 2003. Characterizing and modeling groundwater discharge in an agricultural wetland on the French Atlantic coast. Hydrol. Earth Syst. Sci. 7 (1), 33–42.